# Coprecipitation of Nickel−Copper−Aluminum Takovite as Catalyst Precursors for Simultaneous Production of Carbon Nanofibers and Hydrogen

A. R. Naghash,[†] Z. Xu,*[,†,‡] and T. H. Etsell[†]

*Department of Chemical and Materials Engineering, 536 Chemical and Materials Engineering Building, University of Alberta, Edmonton, Alberta, T6G 2G6, Canada, and Department of Chemistry, South China Normal University, Guangzhou, China 510631*

*Received September 6, 2004. Revised Manuscript Received November 4, 2004*

A series of nickel-, copper-, and aluminum-containing catalysts at a (Ni+Cu)/Al mole ratio of 3 and Cu/Ni mole ratio in the range of 0.03−0.4 was prepared by coprecipitation from corresponding metal nitrate solutions at alkaline pH. The composition and structure of the precipitates were determined by chemical analysis, thermogravimetric analysis (TGA), and X-ray diffraction (XRD). The XRD patterns confirmed that the precipitates are of hydrotalcite-like structures and, more specifically, they are takovite. The brucite-like layers consist of nickel, copper, and aluminum ions of composition $[Cu_yNi_{x-y}Al_{1-x}(OH)_2]^{(1-x)+}$, while the interlayers consist of $CO_3^{2-}$ and crystalline water. The observed variation of lattice parameters with copper content led us to conclude that the copper and aluminum ions were randomly substituted for the nickel ions in the brucite layer. The catalytic conversion tests at 670 °C showed a significantly enhanced catalytic reactivity of 2 mol % copper-doped catalysts as compared to a pristine nickel catalyst. A higher copper doping led to a less significant improvement in catalytic reactivity. A scanning electron micrograph (SEM) confirmed the production of carbon nanofibers.

## Introduction

Research into production of pure hydrogen has been stimulated by the increasing need from refineries for pure hydrogen to produce more reformulated gasolines and deeper hydrotreating diesels.[1] Moreover, the requirement for CO-free hydrogen (at ppm level) becomes even more stringent for its use in proton exchange membrane (PEM) fuel cells.[2] Traditionally, hydrogen is produced by steam reforming or partial oxidation of methane to produce synthesis gas, followed by the water-gas shift reaction to convert CO to $CO_2$.[3−6] The need for CO removal from hydrogen not only increases the complexity of hydrogen production but also sets the economic barrier for its commercialization. It is, therefore, highly desirable to search for other alternatives for production of high-purity hydrogen. Direct thermal decomposition of light hydrocarbons such as methane or ethane via catalytic decomposition may be an alternative route for producing pure hydrogen. In this approach, carbon nanofibers formed during the decomposition as a value added byproduct can have a variety of applications.[7−10] One of the drawbacks in this approach is solid carbon deposition on catalyst during the catalytic reaction, which causes severe catalyst deactivation. Extensive research in the past decade has been devoted to studying and developing new catalysts in an attempt to reduce the severity of carbon deposition during non-oxidative catalytic decomposition of hydrocarbons.

A noncatalytic fossil fuel decarbonization process at temperatures above 800 °C was proposed to produce particulate carbon and hydrogen.[11,12] Bromberg et al.[13,14] studied thermal reforming of natural gas and diesel with and without a catalyst using plasma as the heat source to produce hydrogen in a fuel converter for internal combustion engines. They found that catalyst fouling due to carbon deposition could be avoided by simultaneous purging of reactor with air. In this case, instead of producing solid carbon, gaseous CO is produced as a byproduct. Using impregnation methods, pristine nickel catalyst supported on $Al_2O_3$ or $SiO_2$ was tested for direct cracking of methane or diluted methane. Using a catalyst containing 16 wt % Ni on $SiO_2$ support, an initial methane conversion of 35% was achieved at a reaction

* Corresponding author. Phone: (780) 492-7667. Fax: (780) 492-2881. E-mail: zhenghe.xu@ualberta.ca.
† University of Alberta.
‡ South China Normal University.

(1) Shah, N.; Panjala, D.; Huffman, G. *Energy Fuels* **2001**, *15*, 1528.
(2) Li, Y.; Chen, J.; Qin, Y.; Chang, L. *Enrgy Fuels* **2000**, *14*, 1188.
(3) Rostrup-Nielson, J. R. In *Catalytic Steam Reforming Science and Engineering*; Anderson, J. R., Boudart, M., Eds.; Springer: Berlin, 1984; Vol. 5, p 124.
(4) Rostrup-Nielson, R. J. *Catal. Today* **1993**, *18*, 305.
(5) Armor, J. N. *Appl. Catal.* **1999**, *176*, 159.
(6) Koerts, T.; Deelan, M. J.; Van Santen, R. A. *J. Catal.* **1992**, *138*, 101.
(7) Che, G.; Brinda, B.; Lakshmi, E.; Fisher, R. *Nature* **1998**, *393*, 346.
(8) Gadd, G. E.; Blackford, M.; Moricca, S.; Smith, A. M.; Evans, P. J.; Jacobson, G.; Leung, S.; Day, A.; Hua, Q. *Science* **1997**, *277*, 933.
(9) Iijima, S. *Nature* **1991**, *56*, 354.
(10) Dai, D.; Hafner, G. H.; Rinzler, A. G.; Colbert, D. T.; Smally, R. *Nature* **1996**, *147*, 384.
(11) Steinberg, M. *Int. J. Hydrogen Energy* **1999**, *24*, 771.
(12) Muradov, N. Z. *Energy Fuels* **1998**, *12*, 41.
(13) Bromberg, L.; Cohn, D. R.; Rabinovich, A. *J. Am. Chem. Soc.* **2001**, *123*, 1.
(14) Bromberg, L.; Cohn, D. R.; Rabinovich, A.; Alexeev, N. *Int. J. Hydrogen Energy* **1999**, *24*, 1131.

10.1021/cm048476v CCC: $30.25 
Published on Web 01/21/2005

temperature of 550 °C.[15] The catalyst was found to be deactivated due to spatial limitations imposed on long cylindrical hollow carbon filaments. Choudhary et al.[16] tested catalysts containing 10 wt % Ni on $SiO_2$, H-ZSM-5, and HY zeolite supports for hydrogen production by catalytic decomposition of diluted (20 vol %) methane. The maximum $CH_4$ conversion of 45% at a reaction temperature of 550 °C was reported. The reaction products were found to contain CO and $CO_2$ due to the reaction of the carbonaceous residue with oxygen from oxide supports.

Alloying of catalysts is an alternative to improve catalytic performance by progressively changing the electronic structure of metals in catalysts.[17] Substitution of base metal for noble metals, such as Pt or Pd, makes alloying catalysts more practical for the large-scale applications. Several nickel-based, alloyed catalysts have shown improved catalytic performance by improving their thermal stability during steam reforming, methanation, and direct hydrocarbon cracking.[18,19] $LaNi_5$, for example, was used as a catalyst to produce hydrogen and grow carbon nanotubes by catalytic decomposition of methane at 670 °C.[20] Nanoscale binary Fe−M (where M = Pd, Mo, Ni) catalysts containing 4.5 wt % Fe and 0.5 wt % M supported on $Al_2O_3$ were used for nonoxidative catalytic decomposition of methane at 400−500 °C to produce pure hydrogen and carbon nanofibers.[1] The bimetallic catalysts showed a higher activity than a corresponding monometallic catalyst containing 5 mol % Fe supported on $Al_2O_3$. Alloys of nickel with copper are receiving increasing attention because these two metals form a solid solution. Because copper is less active to chemisorb methane, the optimal doping of copper in a catalyst shows little carbon deposition from aliphatic hydrocarbons at temperatures below 800 °C.[19] To date, most nickel−copper alloys have been made as unsupported metallic powders,[21] films,[22] and single crystals.[23] Little work has been reported on supported nickel−copper alloys prepared by coprecipitation.

The objective of this work is to gain a fundamental understanding of these supported catalysts for direct methane decomposition to produce hydrogen and nanocarbons. The focus of the paper is on the synthesis and characterization of Ni−Cu−Al compounds of hydrotalcite (HT) structure as the precursors of catalysts for simultaneous production of hydrogen and carbon nanofibers from methane decomposition. The synthesis of precursors was performed at pH 7 and 10 with sodium hydroxide and/or sodium carbonate as precipitants. Examined in this study were the effect of calcination temperature on the structure and morphology of oxide samples and the effect of catalyst activation temperature and copper content on catalytic activity.

(15) Zhang, T.; Amiridis, M. D. *Appl. Catal., A* **1998**, *167*, 161.
(16) Choudhary, T. V.; Sivadinarayana, C.; Chusuei, C. C.; Klinghoffer, A.; Goodman, D. W. *J. Catal.* **2001**, *199*, 9.
(17) Dalmon, J. A. *J. Catal.* **1971**, *60*, 325.
(18) Bajpai, P. K.; Bakhshi, N. N.; Liu, D.-C.; Mathews, J. F. *Can. J. Chem. Eng.* **1982**, *60*, 613.
(19) Khulbe, K. C.; Mann, R. S. *Catal. Rev. Sci. Eng.* **1982**, *24*, 311.
(20) Gao, X. P.; Qin, X.; Wu, F.; Liu, H.; Lan, Y.; Fan, S. S.; Yuan, H. T.; Song, D. Y.; Shen, P. W. *Chem. Phys. Lett.* **2000**, *327*, 271.
(21) Sinfelt, J. H.; Carter, J. L.; Yates, D. J. C. *J. Catal.* **1972**, *24*, 283.
(22) Frannken, P. E. C.; Ponee, V. *J. Catal.* **1976**, *42*, 398.
(23) Watanabe, K.; Hashiba, M.; Yamashina, T. *Surf. Sci.* **1976**, *61*, 483.

## Experimental Section

**Sample Preparation.** All of the chemicals (aluminum nitrate, nickel nitrate, cupric nitrate, sodium hydroxide, and sodium carbonate, all from Fisher Scientific) used for catalyst preparation were of analytical grade. The coprecipitation was carried out by mixing two solutions, one containing nickel, aluminum, and cupric nitrates at a (Ni+Cu) to Al mole ratio of 3 and a total metal concentration of 0.4 mol/L, and the other containing a stoichiometric amount of $Na_2CO_3$ and/or NaOH. Initially, 200 mL of distilled water was placed in a 1000 mL beaker equipped with a mechanical stirrer, thermometer and pH probe. The pH was measured with a Fisher 35636-15 pH meter. The prepared solutions (100 mL each) were added simultaneously to the beaker, and the rate of addition was adjusted so that the pH of the mixture was kept constant at a predetermined value by controlled addition of sodium hydroxide and sodium carbonate stock solutions. A number of preparations were carried out by adding $Na_2CO_3$ stock solutions as pH modifier to nitrate solutions to keep the solution at a predetermined pH value. Some of the coprecipitation tests were performed with an ultrasonic dismembrator (Fisher Scientific). The temperature of the solution was maintained throughout at 75−80 °C. Suspensions after precipitation were aged for 15−30 min before the solvent was removed by decanting. The remaining precipitates were rinsed several times with distilled water and acetone to remove sodium ions and residual water, respectively. The cleaned precipitates were then dried under vacuum at 60 °C overnight.

**Characterization.** The prepared precipitates were characterized by X-ray diffraction, chemical analysis, and thermal gravimetric analysis. X-ray diffraction patterns were obtained on a RU 200 diffractometer (Rigaku, Japan) using Cu Kα X-ray as the radiation source. The diffraction patterns were recorded over a $2\theta$ range from 10° to 80° at a step size of 0.05°. Unit cell parameters ($a_o$, $c_o$) were determined by indexing the diffraction peaks according to the hexagonal system with a least-squares fitting program. The nickel, aluminum, and copper content was determined by chemical analysis using a Varian FS 220 atomic absorption spectrophotometer following an aqua-digest method. Thermogravimetric analysis of the formed catalyst precursors was carried out on a Netzsch 409 analyzer under 10 mL $min^{-1}$ flowing air and at a heating rate of 10 °C $min^{-1}$. The particle size of the precursors was measured using a Malvern SM2000 mastersizer. The precipitates were calcined in an up-flow Thermolyne F-21125 vertical furnace with the air flow at 10 mL $min^{-1}$ and a heating rate of 5 °C $min^{-1}$. The calcination temperature varied from 270 to 450 °C for a given period of time.

**Reaction Conditions.** The hydrogen, methane, and nitrogen used in this study were of ultrahigh purity. All of the reactions were carried out in an up-flow vertical reactor. The reaction chamber made of 7.5 mm i.d. quartz tube was heated in the Thermolyne F-21125 furnace. In each test, 80 mg of the calcined catalyst precursor particles was placed in the middle of the furnace where the temperature gradient was small. All of the reactions were carried out under atmospheric pressure. To activate the catalysts, the calcined catalyst precursors were reduced at a given temperature for different periods of time. The reduction was performed under a $H_2$ and $N_2$ gas mixture environment. The $H_2$ to $N_2$ volumetric ratio was fixed at 1/2 with a total gas flow of 27.5 mL $min^{-1}$ (STP). At the end of catalyst activation, the mixed gas was switched to $CH_4/N_2$ at a volumetric ratio of 1/1 and a total gas flow rate of 18.5 mL $min^{-1}$ (STP). The conversion reaction proceeded at a given temperature for 1.5 h. The average methane conversion was calculated by performing a mass balance between the amount of carbon produced (in moles) and the total moles of methane flowing through during the reaction.

**Table 1. Relationship between Chemical Composition and Preparation Parameters**

| sample[a] | reactant | aging (min) | (Ni+Cu)/Al (expected) | (Ni+Cu)/Al (calculated) | Al/(Ni+Cu+Al) (calculated) | size ($\mu$m) |
|---|---|---|---|---|---|---|
| A1 | $NaOH/Na_2CO_3$ | 30 | 3 | 3.2 | 0.24 | 61 |
| A2 | $NaOH/Na_2CO_3$ | 15 | 3 | 2.9 | 0.26 | 36 |
| A3 | $Na_2CO_3$ | 15 | 3 | 3 | 0.25 | 7 |
| B1.8 | $Na_2CO_3$ | 15 | 2.9 | 3 | 0.25 | 7 |
| B3.5u | $Na_2CO_3$ | 15 | 3 | 2.9 | 0.26 | 1 |
| B11u | $Na_2CO_3$ | 15 | 3.1 | 3.1 | 0.24 | 0.7 |
| B22u | $Na_2CO_3$ | 15 | 3 | 2.9 | 0.26 | 2 |

[a] The sample code starting with letter A and B indicates the synthesis without and with Cu doping, respectively. The suffix number reflects the mole percentage of copper in reference to metallic elements used in synthesis. The affix u represents the synthesis performed under ultrasonication. As an example, B3.5u represents a catalyst with 3.5 mol % Cu doped in 97.5 mol % nickel and aluminum, synthesized under ultrasonication.

## Results and Discussion

**Chemical Analysis and Particle Size Determination.** When suitable nickel salt solutions were coprecipitated with aluminum salts, the precipitates formed showed an XRD pattern similar to that of mineral takovite. The chemical formula of takovite is $Ni_6Al_2(OH)_{16}{\cdot}CO_2{\cdot}4H_2O$. The takovite of the hydrotalcite structure[24−28] consists of brucite-like layers, which contain both divalent and trivalent cations in octahedral sites. The brucite layers are separated by disordered interlayers containing water molecules and carbonate ions.

Table 1 summarizes the reaction conditions and actual chemical composition of the formed precipitates. When the synthesis was performed with the addition of NaOH and $Na_2CO_3$, the quantity of $Na_2CO_3$ was chosen in such a way that the ratio of $CO_3^{2-}/(Ni^{2+}+Al^{3+}+Cu^{2+})$ was kept constant at 1/8. The pH in this case is 10; otherwise, it is 7. The results in Table 1 show a significant impact of pH and aging on the average size of the precipitates. At pH 10, the average particle size of the precipitates formed over a short period of aging (15 min) is 36 $\mu$m, which is much smaller than 61 $\mu$m for the precipitates formed over a 30-min aging. At a given aging time (15 min), reducing the coprecipitation pH from 10 to 7 reduced the precipitate size down to 7 $\mu$m. In general, the rate of nucleation is higher at higher pH, because of the higher concentration of hydroxide ions. A rapid precipitation leads to precipitate agglomeration, resulting in a product of larger particle size. The precipitate size can be further reduced to 1−2 $\mu$m by ultrasonicating the solution during the precipitation.

With regard to the type of anions incorporated into the interlayers, it is know that carbonate ions, whenever available, rather than nitrate ions are selectively incorporated into the interlayers.[25,26] At pH < 7, however, nitrate ions could be incorporated into the interlayers due to the lack of carbonate ions. In fact, a very pure hydroxynitrate was obtained when the precipitation was carried out at pH 5.[26] This effect of pH can be accounted for by considering the following chemical equilibria:

$$H_2CO_3 \leftrightarrow H^+ + HCO_3^- \quad (1)$$

$$HCO_3^- \leftrightarrow H^+ + CO_3^{2-} \quad (2)$$

with $pK\alpha_1 = 6.4$ and $pK\alpha_2 = 10.3$. The reactions above show that the carbonate ion concentration in solution is drastically lowered at pH below 6.4 where the carbonate is most likely in the form of $H_2CO_3$. Considering precipitation pH above 7 in our study, the hydroxycarbonates are anticipated to be formed as interlayers of the precipitates.

**Thermogravimetry Analysis (TGA).** Figure 1 shows TGA traces of thermal decomposition in air of samples A1, A2, A3, and B22u. In general, the TGA curves for pristine Ni−Al precipitates are indistinguishable, exhibiting an identical thermal behavior. The weight loss after removal of free water (1.7−2.5%) for pristine nickel precipitates can be divided into two temperature regions: from 100 to 180 °C and from 270 to 350 °C. The first thermal effect amounting to a weight loss of about 7.5% corresponds to the loss of interlayer water, indicating interactions of the water molecules with their surrounding chemical species, such as the intercalated anions and OH groups of the brucite-like layers. The weight loss in the second region is attributed to the total thermal effect of the dehydroxylation of brucite-like layers and depletion of $CO_3^{2-}$, resulting in the collapse of the layer structure. The transition between these two thermal effects depends on many factors, such as mole ratio of cations, type of anions, and the environment of heat treatment.[29] It is reported that the temperature range for the second thermal effect increases with increasing aluminum mole ratio, $x(\simeq Al/(Ni+Al))$.[30,31] Because $x$ values for our pristine nickel precipitates are kept within a very narrow range (0.24−0.26), we anticipate that the temperature range for the second thermal effect remains unchanged as indicated in Figure 1. Moreover, the pH and aging time of precipitation showed little effect on the decomposition of pristine nickel precipitates. This finding indicates that the thermal stability of the formed pristine nickel precipitates does not depend on its preparation conditions. For the samples doped with 22 mol % Cu during preparation (thick line), the second thermal effect occurs over a broader temperature range from 270 to 380 °C, indicating a higher thermal stability of copper-doped precipitates. The information obtained from the above TGA analysis provides us with a guideline for choosing calcination temperatures.

(24) Milliagan, W. O.; Richardson, J. T. *J. Phys. Chem. B* **1955**, *59*, 831.
(25) Bish, D. L.; Brindley, G. W. *Am. Mineral.* **1977**, *62*, 458.
(26) Ingram, L.; Taylor, H. F. W. *J. Min. Soc.* **1967**, *36*, 465.
(27) Ross, G. J.; Kodama, H. *Am. Mineral.* **1967**, *52*, 1036.
(28) Li, Y.; Chen, J.; Chang, L. *Appl. Catal., A* **1997**, *163*, 45.
(29) Pausch, I.; Lohse, H. H.; Schurmann, K.; Allmann, R. *Clays Clay Miner.* **1986**, *34*, 507.
(30) Xu, Z. P.; Zeng, H. C. *Chem. Mater.* **2001**, *13*, 4555.
(31) Xu, Z. P.; Zeng, H. C. *Chem. Mater.* **2001**, *13*, 4564.

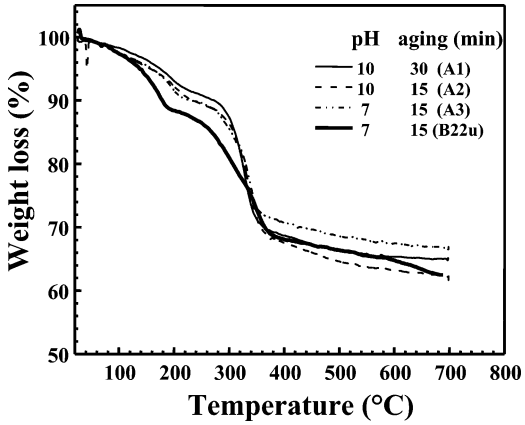


**Figure 1.** Thermogravimetric analysis of pristine- and copper-doped Ni−Al HT-like precipitates.

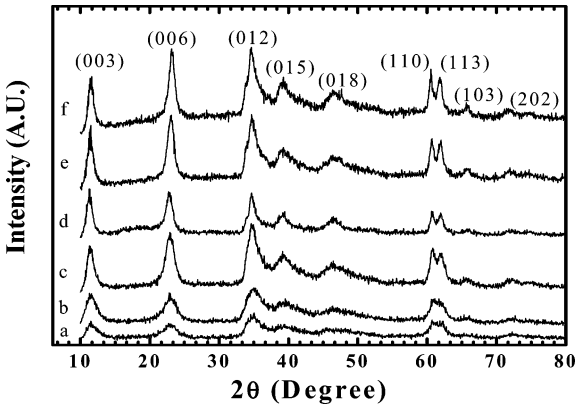


**Figure 2.** X-ray diffraction patterns of Ni−Al HT-like precursors (a) A1, (b) A2, (c) A3, (d) B1.8, (e) B11u, and (f) B22u.

**Structural Analysis.** Figure 2 shows X-ray diffraction patterns (XRD) of the freshly prepared and dried pristine and copper-dopd Ni−Al precipitates. The XRD patterns obtained are characteristic of those for HT-like minerals and could be indexed on a rhombohedral base of 3R symmetry. The unit cell parameters of a rhombohedral structure are $a_o$ and $c_o = 3c'$, where $c'$ is the thickness of one layer constituting a brucite-like sheet and one interlayer.[32,33] There is no sign of additional peaks for a second phase, indicating the absence of any other nickel-, aluminum-, or copper-containing phases in the precipitates. Generally speaking, the pristine Ni−Al is of HT-like structure when the mole fraction of aluminum, $x$, is within 0.2−0.4.[34−36] Copper-doped Ni−Al is also of HT-like structure when the Cu to Ni molar ratio is equal to or lower than 1. It is known that $Cu^{2+}$ ions are situated in octahedras of brucite layers. Due to the Jahn−Teller effect, the presence of $Cu^{2+}$ in the HT lattice of pristine Ni−Al precipitates will cause a distortion of the octahedral coordination, leading to a gain of lattice energy. When the $Cu^{2+}/Ni^{2+}$ mole ratio is higher than 1, this distortion becomes so severe that the formation of other copper-containing phases become energetically more favorable. Because our actual $x$ value is 0.25 and the copper to nickel mole ratio ranges from 0.03 to 0.4, the absence of other phases other than HT is not unexpected, as confirmed by XRD patterns shown in Figure 2.

**Table 2. Lattice Parameter ($a_o$), Interlayer Spacing ($^1/_3c_o$), and Chemical Formula of the Pristine- and Copper-Doped Samples**

| sample | $a_o$ (Å) | $^1/_3c_o$ (Å) | chemical formula |
|---|---|---|---|
| A3 | 3.04 | 7.71 | $Ni_{0.75}Al_{0.25}(OH)_2 \cdot 0.125CO_3 \cdot 0.5H_2O$[a] |
| B1.8 | 3.04 | 7.70 | $Ni_{0.732}Cu_{0.018}Al_{0.25}(OH)_2 \cdot 0.125CO_3 \cdot 0.5H_2O$ |
| B3.5u | 3.05 | 7.63 | $Ni_{0.705}Cu_{0.035}Al_{0.26}(OH)_2 \cdot 0.13CO_3 \cdot 0.52H_2O$ |
| B11u | 3.06 | 7.75 | $Ni_{0.65}Cu_{0.11}Al_{0.24}(OH)_2 \cdot 0.12CO_3 \cdot 0.48H_2O$ |
| B22u | 3.09 | 7.65 | $Ni_{0.52}Cu_{0.22}Al_{0.26}(OH)_2 \cdot 0.13CO_3 \cdot 0.52H_2O$ |

[a] Interlayer water is based on a $CO_3^{2-}$ to $H_2O$ stoichiometry ratio of 1/4.

As compared to samples A1 and A2 (synthesized at pH 10), sample A3 (synthesized at pH 7) was much better crystallized, as is evidenced by much narrower X-ray diffraction peaks of higher signal-to-noise ratio. Moreover, for samples A1 and A2, the (0$kl$) diffraction peaks ((012), (015) and (018)) are broad and asymmetric, indicating stacking disorder.[37,38] This observation appears to be in line with the discussions above, that the rate of nucleation is higher than crystal growth at higher pH, causing the formation of less crystalline precipitates. At pH 7, the above (0$kl$) diffractions become much better developed and more symmetrical with increasing copper doping. Moreover, the separation of the two peaks at $2\theta = 60.7$ and 62.1 becomes more pronounced as the copper content increases, indicating a better crystallized structure for copper-doped samples. The improved crystallinity with increasing copper doping accounts for the observed improvement of thermal stability shown in TGA tests. In all of the cases, the positions of these (0$kl$) diffraction lines are in excellent agreement with indexing of a tripled $c$-axis, that is, 3 times the distance between the layers of metal ions. This is of the same stacking sequence as in the rhombohedral mineral hydrotalcite.

Table 2 summarizes the lattice parameters $a_o$ and $c_o$ and the chemical formula of the samples (based on chemical analysis) as a function of copper content. The layer spacing ($^1/_3c_o$ or $c'$) for copper-doped samples does not change significantly with an increase in the copper content. This is in line with a close match of ionic radii between copper and nickel ($Ni^{2+} = 0.83$ Å, $Cu^{2+} = 0.87$ Å). Gastuche et al.[37] observed a decrease in layer spacing with an increase in the amount of $Al^{3+}$. This was explained by the increase in electrostatic attraction between the brucite layer and interlayer due to a higher positive charge of $Al^{3+}$. The slight change in interlayer spacing for pristine- and copper-doped samples is due to a slight change in $Al^{3+}$ content as can be seen for samples B3.5u, B11u, and B22u in Table 2. The $a_o$ parameter is a measure of the average M−M (Ni, Al, Cu) distance in the basal plane of the rhombohedral structure. The monotonic increase in the $a_o$ parameter with increasing copper content is consistent with an increase in the presence

(32) Allmann, A. *Chimia* **1970**, *24*, 99.
(33) Drits, A.; Sokolova, T. N.; Sokolova, G. V.; Cherkashin, V. I. *Clays Clay Miner*. **1987**, *35*, 401.
(34) Brindley, G. W.; Kikkawa, S. *Am. Mineral*. **1979**, *64*, 836.
(35) Gherardi, P.; Ruggeri, O.; Trifiro, F.; Vaccari, A.; Del Piero, G.; Manara, G.; Notari, B. In *Preparation of Catalysts III*; Poncelet, G., Grange, P., Jacobs, P. A., Eds.; Elsevier: Amsterdam, 1983; p 723.
(36) Busetto, C.; Del Piero, G.; Manara, G.; Trifiro, F.; Vaccari, A. *J. Catal*. **1984**, *85*, 260.
(37) Gastuche, M. C.; Brown, G.; Mortland, M. M. *Clays Clay Miner*. **1967**, *7*, 177.
(38) Brown, G.; Gastuche, M. C. *Clays Clay Miner*. **1967**, *7*, 193.

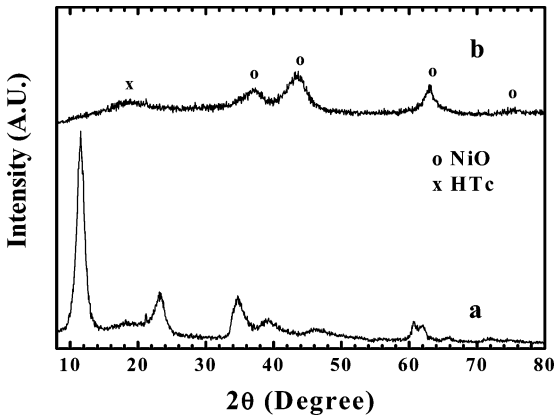


**Figure 3.** X-ray patterns of nickel catalyst precursors containing 1.8 mol % Cu: (a) as synthesized, and (b) after heat treatment at 270 °C for 17 h.

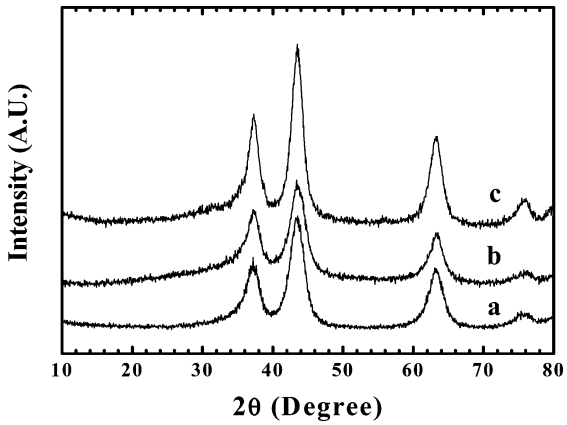


**Figure 4.** X-ray diffraction patterns of calcined catalyst precursors heat-treated at 450 °C for 2 h after 17-h heat treatment at 270 °C: (a) pristine nickel, (b) doped with 1.8 mol % Cu, and (c) doped with 11 mol % Cu.

of slightly larger $Cu^{2+}$ cations in the lattice, especially at higher copper content.

The results in Table 2 are best explained on the basis of hydrotalcite structure in which the nickel, copper, and aluminum cations are incorporated in brucite-type hydroxide layers that have the chemical composition of $[Cu_yNi_{x-y}Al_{1-x}(OH)_2]^{(1-x)+}$. The $CO_3^{2-}$ is incorporated between the layers (interlayers) to compensate for the excess charge of the layers, caused by the presence of aluminum cations. Water is also included in the crystal structure of the interlayer. The main evidence for the incorporation of the aluminum and copper ions in the brucite layers comes from the observation (Table 2) that the $^1/_3c_o$ value decreases with increasing aluminum content and the $a_o$ parameter increases with increasing copper content.

**Calcined Samples.** In the preparation of Ni−Al mixed oxide catalysts from Ni−Al HT-like precursors, selecting the type of anions is critical. Sulfate anions $(SO_4)^{2-}$ could departure as $SO_3$ gases during calcination only at temperatures above 850 °C.[27] Nitrate ions promote sintering of NiO crystallites during calcination at high temperatures. In the case of chlorine, it not only enhances the sintering of NiO particles, but also remains bonded to the nickel, poisoning the reactivity of the resultant catalysts. Among the available anions, carbonates are considered as the best anion for the preparation of pristine- or copper-doped Ni−Al HT-like catalysts, as carbonate can departure as $CO_2$ at relatively low calcination temperatures.

Figure 3 shows the XRD patterns of B1.8 precursors before and after heat treatment at 270 °C for 17 h. This calcination temperature was chosen on the basis of the thermogravimetric analysis results which indicated dehydroxylation starting at 270 °C. After 17 h at 270 °C in air, three distinct diffraction peaks at $2\theta = 37°$, 44°, and 62° in Figure 3b were observed. These peak positions correspond well with three most intense peaks of NiO in JCPDS 78-0643, indicating the formation of a cubic NiO phase at this calcination temperature. When the sample was heat-treated at this temperature for only 6 h, XRD patterns corresponding to NiO were not observed. This observation indicates that the total decomposition to nickel oxide could be accomplished at lower temperatures (270 °C) than that indicated by thermogravimetric analysis (350−380 °C), provided that a sufficient calcination time is allowed.

Figure 4 shows the XRD patterns of samples A3, B1.8, and B11u, which were heat-treated for an additional 2 h at 450 °C after initial heat treatment at 270 °C for 17 h. In this case, the diffraction patterns are identical to that shown in Figure 3b, except that the diffraction patterns become much sharper, indicating a product of much higher crystallinity. Also interesting to note is that even at 11 mol % copper doping, the diffraction pattern (Figure 4c) remains characteristic of single-phase NiO, indicating the absence of CuO or $Al_2O_3$ as second phases. From this study, the heat treatment in air at 270 °C for 17 h followed by 450 °C for 2 h was established to form the desired copper-doped Al-containing NiO crystal structure.

**Catalyst Activation and Reactivity.** When the carbonate form of the Cu−Ni−Al HT-like compound is calcined at a temperature above that necessary for complete destruction of the layer structure, the neighboring nickel, copper, and aluminum cations in the layer are redistributed. This redistribution gives rise to a nickel oxide-rich phase in which copper and aluminum oxides are dissolved. The XRD patterns show that the activation under a reducing ($H_2$) environment of such a phase results in a uniform distribution of copper and nickel on aluminum oxide support. No XRD peaks corresponding to alumina have been observed. It is believed that under the hydrogen reduction condition at 700 °C for 1.5 h, the long-range order of $Al^{3+}$ cations may not be accomplished. The activated catalysts are used in catalytic decomposition of methane for simultaneous production of hydrogen and carbon nanofibers. In this paper, only preliminary results of catalytic conversion with activated catalysts are presented. A more systematic investigation of the simultaneous production of hydrogen and carbon nanofibers will be given in a separate paper.

To understand the reducibility of copper-doped nickel oxide catalysts, samples A3, B3.5u, and B11u after calcination were subjected to TGA tests under hydrogen purge at atmospheric pressure. For comparison, unsupported pristine CuO was also tested under the identical conditions. The results are shown in Figure 5. For the convenience of discussion, the weight loss curves in Figure 5a are differentiated with respect to temperature to result in corresponding differential weight loss (DWL) curves as shown in Figure 5b. It should be noted that the weight loss of the samples up

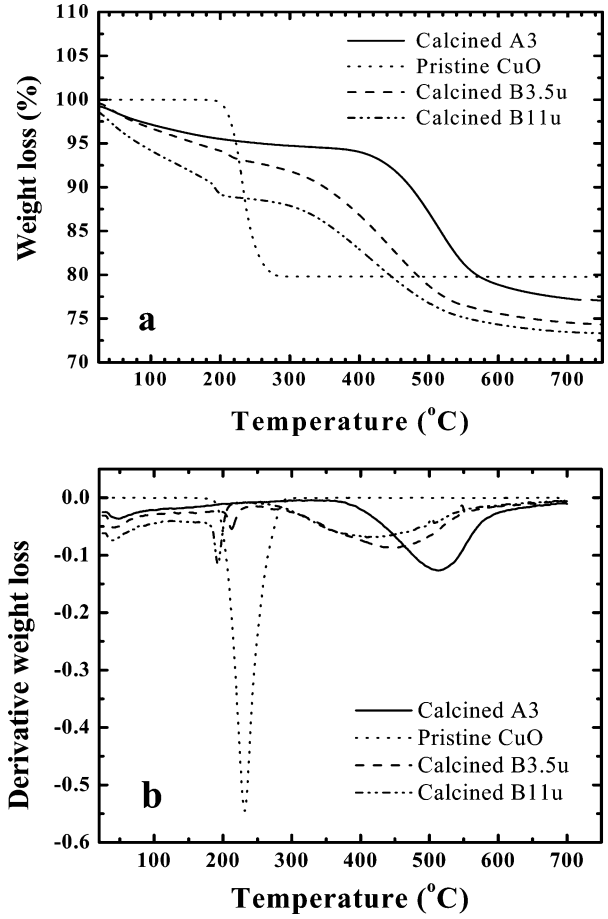


**Figure 5.** Reduction reaction profiles (a) and corresponding derivative weight loss (b) of copper−nickel−aluminum oxides heat-treated at 450 °C for 2 h after 17-h heat treatment at 270 °C and unsupported pristine copper oxide.

to 100 °C is a result of free water removal. For the A3 sample of NiO containing 25 mol % Al, the weight loss during reduction started at 400 °C and ended at about 600 °C (Figure 5a), exhibiting a broad DWL peak at 500 °C. A weight loss of unsupported pristine NiO between 300 and 500 °C and a peak at 430 °C on DWL[28] was reported as a result of NiO reduction to metallic nickel. The similarity between our thermal analysis results and those reported in the literature suggests reduction of NiO to nickel. However, the temperature at which the peak appeared on DWL is substantially higher in our study than that for the reduction of unsupported pristine NiO mentioned above, illustrating a greater difficulty of NiO reduction in solid solution as in A3 catalyst than in unsupported pristine NiO. Strong interactions between nickel and aluminum ions in solid solution appear to cause a shift to higher activation temperatures, as observed in our study.

For unsupported pristine CuO, the rapid weight loss started at 200 °C and ended at 275 °C, with the peak of DWL at about 230 °C. This temperature range of reduction is much lower than that for both unsupported pristine NiO[28] and A3 sample, suggesting that CuO is reduced more readily than NiO. This finding is important when interpreting the TGA results for copper-doped nickel catalysts.

The reduction profile of 3.5 mol % copper-doped nickel−aluminum samples (B3.5u) exhibits two distinct temperature ranges of significant weight losses. The first weight loss occurred between 200 and 220 °C with the peak of DWL at

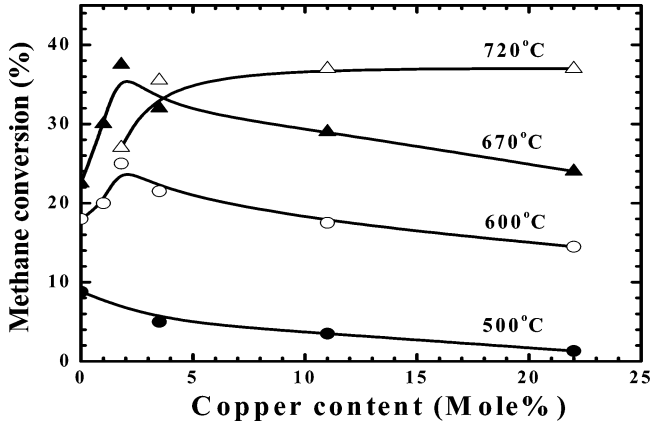


**Figure 6.** Catalytic activity plot for methane decomposition as a function of copper content and temperature of reaction.

around 190 °C. The weight loss here accounts for the reduction of copper ions. The second weight loss started at around 300 °C and ended at around 550 °C with the peak of DWL at around 450 °C. This weight loss is attributed to the reduction of nickel ions. The 11 mol % copper-doped sample (B11u) showed reduction profiles similar to those of sample B3.5u, except that the weight loss profiles are shifted toward lower temperature directions. A careful examination of Figure 5 led us to conclude that copper tends to be selectively reduced at lower reduction temperatures and the presence of copper lowers the reduction temperature of nickel. The reduction of nickel ions at lower temperature in the present of copper may be explained by considering the creation of cation and anion vacancies after reduction of $Cu^{2+}$. The decrease of ionic interactions among surrounding nickel ions due to creation of these vacancies allows nickel to be reduced at lower temperatures. A similar effect has been utilized in many metal catalysts for the purpose of reducing catalyst activation temperatures.[39]

Figure 6 shows the effect of reaction temperature on methane conversion for pristine- and copper-doped nickel catalysts. The catalysts are activated at 700 °C under a mixture of hydrogen and nitrogen (at a 1:2 volumetric ratio) environment for 90 min. From this figure, methane conversion is seen to decrease with increasing copper concentration in catalysts. This general trend is more prominent at reaction temperatures between 500 and 700 °C. At reaction temperatures below 500 °C, the overall methane conversion is low for all of the catalysts prepared. The SEM morphology study showed that solid carbons formed at this temperature were not fibrils. It is evident that the highest conversion (37%) was obtained at a reaction temperature of 670 °C using catalysts doped with 1.8 mol % Cu. More importantly, under such reaction conditions, the carbons formed are mostly fibrils (Figure 7a), whereas using pristine nickel catalysts, the carbons formed are plateaus (Figure 7b). The TEM micrograph in the inset of Figure 7a shows a clear view of carbon nanofibers after acid washing. These carbon nanofibers are of relatively uniform sizes. The width of the nanofibers in the range of 35−40 nm normally represents the grain size of the catalysts, observed at the end of carbon

(39) Khulbe, K. C.; Mann, R. S. *Catal. Rev. Sci. Eng.* **1982**, *24*, 311.

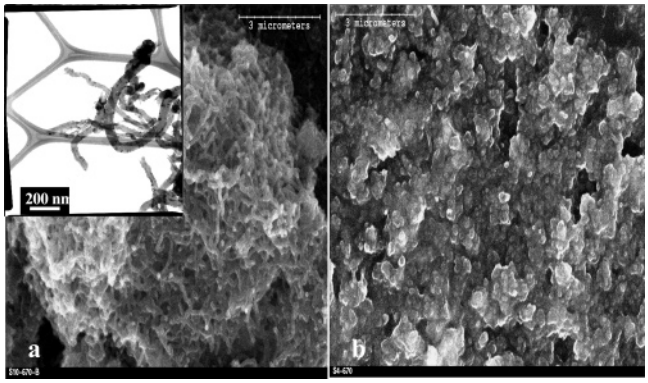


**Figure 7.** SEM micrographs of: (a) carbon nanofibers on 1.8 mol % Cu-doped Ni catalyst, and (b) plateaus of carbon on pristine Ni catalyst, both formed at 670 °C. The inset of (a) is a TEM micrograph magnifying carbon nanofibers shown in (a).

nanofibers in our TEM micrograph before acid washing (not shown here). Moreover, these nanofibers are of straight herringbone type, each with a catalyst particle located at its free end. These observations suggest a growth mechanism of carbon nanofibers on catalyst grains and emphasize a means of controlling carbon nanofiber diameters by controlling the grain size of catalysts. This morphology is in great contrast to octopus-like nanofibers attached to the same metallic particle. The octopus-like nanofibers are produced when polyhedral metal particles are formed during catalyst activation.[40]

Reducing copper doping to 1 mol %, on the other hand, caused a lower methane conversion but remained higher than that of pristine nickel catalysts. More importantly, the carbons formed under these conditions were plateaus rather than fibrils. At a reaction temperature of 720 °C, the methane conversion increased only when catalysts B11 and B22 were used. For catalysts A3 and B1.8, methane conversion at 720 °C was lower than that at 670 °C. The results reported here suggest that the best performance of the catalyst may be obtained by doping the pristine nickel with ∼2 mol % copper with a methane conversion at 670 °C.

It is well documented that copper is inactive in catalyzing decomposition of methane to carbon and hydrogen.[41] It appears that the doping of a small amount of copper into nickel catalysts reduces the rate of carbon formation by reducing the rate of conversion. The reduction in surface concentration of carbon on the catalyst promotes the carbon diffusion into the nickel catalyst as opposed to the formation of C−C bonding on the catalyst surface under the conditions of high carbon surface concentration. The carbon diffusion into the catalyst promotes carbon filament growth and, at the same time, generates active surface sites for dehydrogenation of subsequent methane molecules. As a result, a small amount of copper doping in supported nickel catalysts favors the formation of carbon nanofibers (Figure 7) and increases the catalyst's lifetime by minimizing rapid catalyst deactivation. However, excessive copper doping of the supported nickel catalysts will reduce the available active sites for methane decomposition and hence overall conversion. More systematic experiments are needed to fully understand the role of copper doping in controlling simultaneous production of hydrogen and carbon nanofibers. The kinetics of carbon formation has been studied on copper−nickel single crystals and foils.[22] A similar approach could be applied to the study of supported copper−nickel catalysts to establish a correlation between the copper content in the doped catalysts and the rate of methane decomposition in the context of carbon nanofiber formation. The study on this aspect is currently underway.

## Conclusions

The results described in this paper demonstrated the synthesis of Cu−Al-doped nickel catalysts by coprecipitation from a copper−nickel−aluminum nitrate solution, for the simultaneous production of carbon nanofibers and hydrogen from methane. Single-phase precipitates of the hydrotalcite-like layer structure were obtained when synthesis was performed with an aluminum mole fraction ($x_{Al}$) of 0.25 and a copper mole fraction ($x_{Cu}$) in the range of 0−0.22, balanced with nickel. The size of the precipitates was found to be greatly affected by precipitation pH. Low-temperature calcination for a long period of time followed by heat treatment at moderate temperatures for a short period time was found to favor the formation of single-phase nickel oxide, a desired product as catalyst precursors. A 1.8 mol % copper doping was found to be optimal for methane conversion at 670 °C and carbon nanofiber formation. A further increase in copper doping reduced methane conversion. The features of the solid carbon formed depend on both the level of copper doping and the methane conversion temperatures.

**Acknowledgment.** The financial support for the present work from the Natural Sciences and Engineering Research Council (NSERC), Edmonton Power Corporation (EPCOR), the Alberta Energy Research Institute (AERI) under the NSERC/EPCOR/AERI Industrial Research Chair program, and the COURSE research program is greatly appreciated.

CM048476V

(40) Chen, J.; Li, X.; Li, Y.; Qin, Y. *Chem. Lett.* **2003**, *32*, 424.
(41) Tavares, M. T.; Alstrup, I.; Bernardo, C. A.; Rostrup-Nielsen, J. R. *J. Catal*. **1996**, *158*, 402.